CHAPTER 4
PERTURBATIONS OF NONLINEAR RESONANCES — TUNE MODULATION AND BETA MODULATION

The effects of various types of perturbations on particle motion influenced by an isolated nonlinear resonance are investigated in this chapter. Two types of perturbation are of particular interest here: modulation of the machine tune and modulation of the linear beta functions at the nonlinear magnets driving the resonance.

Modulation effects are important for a variety of reasons. From a general dynamic viewpoint, the separatrices surrounding nonlinear resonance islands are extremely fragile under small perturbations such as modulations because they are homoclinic, or asymptotically joined to the unstable fixed points of the resonances (Lichtenberg and Lieberman 1983, Vivaldi 1984). As the modulation strength grows motion becomes stochastic in a widening area around the separatrix; this stochasticity can then act as a noise source for diffusion models that may be important mechanisms limiting the luminosity lifetimes of present and future colliders. One of these diffusion models, aptly named modulational diffusion, is described in greater detail in Chapter 7. Tune modulation is also important in study of the beam-beam interaction where its inclusion is necessary to reconcile operational observations with simulation and theory (Peggs and Talman 1986, Saritepe and Peggs 1991). Modulation methods have been proposed for use in crystal channeling and parasitic beam extraction at the SSC (Gabella et. al. 1992) where controlled RF modulation would be used to create trapping resonances in longitudinal phase space.

Most importantly from the perspective of this dissertation, modulations pro-

vide a frequency-dependent mechanism for detrapping particles captured within nonlinear resonance islands. This allows measurement of the island tune Q_{I} even in the experimental circumstance of large beam sizes. It is the objective of this chapter to describe this mechanism within the discrete Hamiltonian context and to summarize the requirements for both tune modulation and beta modulation to detrap particles captured near the resonance island fixed points.

The general character and sources of tune modulation and beta modulation are described in § 4.1. The one-dimensional driven pendulum N-turn Hamiltonian with tune modulation is derived in § 4.2, and the corresponding equations of motion are developed. In § 4.3 we explore the structure of the tune modulation parameter space (q, Q_M) and find four dynamical regions of interest — the adiabatic "amplitude-modulation" region, the fast-modulation "phase-modulation" region, the "strong-sideband" region and a region of chaos where the regular local motion around the fixed points vanishes. We investigate the effects of beta modulation in the N-turn Hamiltonian and compare them to those of tune modulation in § 4.4, and compare the theoretical predictions of the previous sections to particle tracking for both modulations in § 4.5.

4.1 SOURCES OF TUNE MODULATION AND BETA MODULATION

If Q_0 denotes the unperturbed tune, tune modulation is assumed to be of the form

$$Q_0 \rightarrow Q_0 + q \sin(2\pi Q_M t) \; . \tag{4.1}$$

The tune modulation strength, or depth, is q, and Q_M is the modulation frequency; both are frequency-domain parameters and are expressed in inverse turns. This type of tune modulation unavoidably arises from two sources: ripple on quadrupole power supplies and coupling of synchrotron oscillations to the tunes via

chromaticity. The latter is normally the more important source due to the conservative bounds placed on power supply current ripple, on the order of $\Delta I/I \approx 10^{-5}$ to stabilize machine tunes to 10^{-3} accuracy.

With typical chromaticities of several units and fractional momentum offsets δ of about 10^{-4}, Equation (2.19) shows that modulation strengths q of approximately 10^{-3} are always present in the Tevatron. The modulation frequency for these oscillations is the synchrotron frequency, ranging from $1.4 \cdot 10^{-3}$ at injection to $5.7 \cdot 10^{-4}$ at collision energies. It is difficult to reduce the momentum spread of the beam, both because of demands on RF systems and because of coupled bunch instabilities that appear at high longitudinal beam densities. Reduction of chromaticities ξ is also impractical because chromaticities much smaller than a few units can cause strong head-tail instabilities in individual beam bunches.

Tune modulation can also be explicitly introduced by modulating the power supply currents of a set of quadrupole correctors. A modulated quadrupole error of strength $\Delta\tilde{b}_1$ at a location with horizontal beta function $\beta_x(\text{quad})$ will modulate the horizontal tune vis. Equation (2.22):

$$q = \frac{\Delta\tilde{b}_1 \, \beta_x(\text{quad})}{4\pi} \, . \tag{4.2}$$

The vertical tune is modulated with an opposite sign (completely out of phase from the horizontal) using the corresponding beta function. Discussion of controlled modulation for the E778 tune modulation experiment is deferred until Chapter 5.

Quadrupole modulation not only changes the tune of the machine but also modulates the beta functions around the ring. Quantitatively the amplitude $b(s)$ of this beta modulation,

$$\beta \rightarrow \beta \left[1 + b(s) \sin(2\pi Q_M t)\right] \, , \tag{4.3}$$

is given by Sands (Sands 1970, eq. [2.105]):

$$b(s) \equiv \frac{\Delta\beta(s)}{\beta(s)} = \frac{2\pi q}{\sin(2\pi Q_0)} \cos[2|\psi(s) - \psi(\text{quad})| - 2\pi Q_0] \, . \tag{4.4}$$

The only longitudinal position dependence is in the cosine; this perturbation causes a so-called "beta wave" around the accelerator with a cusp at the location of the quadrupole error. Examination of the first-order nonlinear Hamiltonians Equations (3.6) and (3.7) shows that, for the single resonance term $\cos(N\psi)$ selected by N-turn summation, the final effect of beta modulation is, to first order in b, a modulation of the resonance strength:

$$V_N \rightarrow V_N \left[1 + \frac{Nb}{2}\sin(2\pi Q_M t)\right] \ . \tag{4.5}$$

The beta modulation strength in Equation (4.4) is expressed in terms of the tune shift for the quadrupole to compare the relative effectiveness of tune and beta modulation in detrapping particles captured within nonlinear resonance islands. For a single quadrupole error the maximum beta modulation amplitude b is roughly an order of magnitude larger than the corresponding tune modulation depth q; for a set of modulated quadrupoles distributed in phase $\psi(s)$ (as used in E778) interference between beta waves from individual quadrupoles makes this ratio about two to three times smaller.

A similar, though not equivalent, modulation is produced by synchrotron oscillations of a particle with nonzero fractional momentum offset δ. These modulate the magetic rigidity $|B\rho| \rightarrow |B\rho|\,[1 + \delta\sin(2\pi Q_M t)]$, effectively modulating the normalized multipole strengths. For $\delta \ll 1$, always the case in realistic operations,

$$\tilde{b}_n \rightarrow \tilde{b}_n[1 - \delta\sin(2\pi Q_M t)] \tag{4.6}$$

to first order in δ. This modulates the resonance strength V_N differently than beta modulation does, since here V_N is proportional to $\tilde{b}_n$ in a first-order nonlinear analysis:

$$V_N \rightarrow V_N[1 - \delta\sin(2\pi Q_M t)] \ . \tag{4.7}$$

So $b = 2\delta/N$ for beta modulation induced by synchrotron oscillations.

4.2 THE N–TURN HAMILTONIAN FOR TUNE MODULATED ONE–DIMENSIONAL RESONANCES

We begin with the one-turn one-dimensional Hamiltonian of Equation (3.13), including tune modulation:

$$H_1(\psi, J; t) = 2\pi Q_0 J + \frac{1}{2}\alpha J^2 + V_N J^{N/2}\cos(N\psi) + 2\pi q J \sin(2\pi Q_M t) \ . \qquad (4.8)$$

The single resonance term is the only one kept because all others, not of interest in an isolated resonance model, are suppressed in the summation used to produce an N-turn Hamiltonian. The tune is again assumed to be near the resonant tune, $Q_0 = \frac{M}{N} + \delta_Q$ where $\delta_Q \ll \frac{1}{N}$. We shall consider only tune modulation frequencies Q_M much smaller than $1/N$ so the tune is adiabatically changing over these N turns, and tune modulation depths $q \lesssim \delta_Q$. Real sources of tune modulation described in the previous section agree with these limits; much larger tune modulation strengths prohibit any regular motion with strongly driven resonances. The one-turn Hamiltonian is now summed over N turns as in the previous chapter to give, to first order in the small strengths α, V_N and q:

$$\begin{aligned} H_N(\psi, J; T) = {} & 2\pi N\delta_Q J + 2\pi N q J \sin(2\pi N Q_M T) + \frac{N}{2}\alpha J^2 \\ & + N V_N J^{N/2}\cos(N\psi) \ . \end{aligned} \qquad (4.9)$$

The N-turn Hamiltonian can exhibit fixed points as before for certain sections of the modulation parameter space (q, Q_M). Solving the equation $\dot{J} = 0$ for the fixed point phases gives $\phi_{fp} = 0, \pi/N, \ldots (2N-1)\pi/N$. Similarly, solving $\dot{\psi} = 0$ for the fixed point actions gives

$$\begin{aligned} 0 &= 2\pi\delta_Q + 2\pi q \sin(2\pi N Q_M T) + \alpha J_{fp} \ , \\ \dot{J}_{fp} &= -\frac{4\pi^2 N}{\alpha} q Q_M \cos(2\pi N Q_M T) \ . \end{aligned} \qquad (4.10)$$

We transform the coordinates to the small action-angle coordinates (θ, I), expanded around a stable fixed point, via the linear transformations of the previous

chapter —

$$\begin{aligned} \phi &= \frac{\pi}{N} + \theta \ , \\ J &= J_{fp}(T) + I \ . \end{aligned} \tag{4.11}$$

This transformation also changes the Hamiltonian because it is nonautonomous, or time-dependent:

$$H_N(\psi, J; T) \rightarrow H_N(\theta, I; T) + \theta \dot{J}_{fp} \ . \tag{4.12}$$

Performing this change of coordinates produces a driven pendulum Hamiltonian,

$$H_N(\theta, I) = \frac{N}{2}\alpha I^2 + N V_N J_{fp}^{N/2} \cos(N\theta) - \frac{4\pi^2 N}{\alpha} q Q_M \theta \cos(2\pi N Q_M T) \ , \tag{4.13}$$

The equation of motion of the angle variable θ becomes that of a pendulum, driven at the modulation frequency Q_M:

$$\ddot{\theta} = -N(2\pi Q_{\rm I})^2 \sin(N\theta) - 4N^2\pi^2 q Q_M \cos(2\pi N Q_M T) \ . \tag{4.14}$$

This form agrees with others previously published (Peggs 1988, Chen 1990) if the timescale is changed back to single turns via $T \rightarrow t/N$.

When the equation of motion for the angle θ is linearized, it can be solved easily and explicitly for $\theta(T)$. The solution is found to be

$$\theta(T) = \frac{q}{Q_M} \frac{Q_M^2}{Q_M^2 - Q_{\rm I}^2} \cos(2\pi Q_M N T) \ . \tag{4.15}$$

From the Hamiltonian we can also get the solution for the action I as a function of T, since $\dot{\theta} \approx N\alpha I$:

$$I(T) = \frac{2\pi q}{\alpha} \frac{Q_M^2}{Q_{\rm I}^2 - Q_M^2} \sin(2\pi Q_M N T) \ . \tag{4.16}$$

4.3 STRUCTURE OF THE (q, Q_M) PARAMETER SPACE

From the structure of the driven pendulum equation of motion, it is natural to investigate the structure of the (q, Q_M) modulation parameter space. Rescaling

the time by $T \to T/Q_{\rm I}$ in Equation (4.14) shows that the natural scaling for both q and Q_M is $Q_{\rm I}$, since only the ratios $q/Q_{\rm I}$ and $Q_M/Q_{\rm I}$ appear under this scale change:

$$\ddot{\theta} = -N(2\pi)^2 \sin(N\theta) - 4N^2\pi^2 \left(\frac{q}{Q_{\rm I}}\right)\left(\frac{Q_M}{Q_{\rm I}}\right) \cos\left[2\pi N \left(\frac{Q_M}{Q_{\rm I}}\right) T\right] \ . \qquad (4.17)$$

It is interesting to look at three extremes of the parameter space: when $Q_M \ll Q_{\rm I}$ (adiabatic modulation), $Q_M \gg Q_{\rm I}$ (fast modulation) and $Q_M \approx Q_{\rm I}$ (resonance).

First consider the case of adiabatic tune modulation, where the modulation tune is much smaller than the island tune, or many particle oscillations take place around the fixed point with every modulation cycle. Here we can consider the tune to be changing linearly with a small rate of $\dot{Q} = dQ/dT$. The transformed Hamiltonian of Equation (4.13) is now given by

$$H_N(\theta, I; T) = \frac{N}{2}\alpha I^2 + NV_N J_{fp}^{N/2} \cos(N\theta) + 2\pi\dot{Q}TI \ . \qquad (4.18)$$

The dependence on $\dot{Q}T$ may be relegated to second order with the generating function

$$G(I, \bar{\theta}; T) = -I\bar{\theta} + \frac{2\pi\dot{Q}}{\alpha} T\bar{\theta} \ , \qquad (4.19)$$

which gives the transformations $\bar{I} = I - 2\pi\dot{Q}T/\alpha$ and $\theta = \bar{\theta}$. The new Hamiltonian is now no longer periodic in the angle variable $\bar{\theta}$, for it becomes

$$H_N(\bar{\theta}, \bar{I}) = \frac{N}{2}\alpha \bar{I}^2 + NV_N J_{fp}^{N/2} \cos(N\bar{\theta}) + \frac{2\pi\dot{Q}}{\alpha}\bar{\theta} \ . \qquad (4.20)$$

This Hamiltonian *explicitly* modulates the pendulum amplitude $\bar{I}$, as can be seen by the Hamilton's equation for it's rate of change:

$$\dot{\bar{I}} = -\frac{\partial H_N}{\partial \bar{\theta}} = N^2 V_N J_{fp}^{N/2} \sin(N\bar{\theta}) + \frac{2\pi\dot{Q}}{\alpha} \ . \qquad (4.21)$$

Now there are only angle fixed points if we can find $\bar{\theta}_{fp}$ such that $\dot{\bar{I}} = 0$. Noting that the maximum value of the rate of change of the tune is $\dot{Q}_{max} = 2\pi N q Q_M$,

we find the constraint

$$\left| \frac{q}{Q_{\rm I}} \frac{Q_M}{Q_{\rm I}} \right| < \frac{1}{N} \tag{4.22}$$

for adiabatic stability over the entire modulation sweep. As has been previously mentioned (Peggs 1988, Chao and Month 1974), this is an analogue to RF bucket shrinkage during particle acceleration. The above procedure is equivalent to transforming the original N-turn Hamiltonian (4.9) via a generating function that modulates only the action (or amplitude),

$$G(\psi, I; T) = [J_{fp}(T) + I][\psi - k_{res}\pi] \; ; \tag{4.23}$$

hence this region is dominated by "amplitude modulation", where the modulation predominantly modulates island amplitudes instead of island phases as mentioned above.

Second, consider the "fast modulation" case, where $Q_M \gg Q_{\rm I}$. As might be expected from the above comments, this region is dominated by "phase modulation." Consider transforming to the phase-modulated fixed points with application of the generating function

$$G_2(\psi, I; T) = [J_{fp} + I][\psi - \psi_{fp}(T)] \tag{4.24}$$

to the N-turn Hamiltonian (4.9) — this produces

$$H_N(\theta, I) = \frac{N}{2}\alpha I^2 + 2\pi N q I \sin(2\pi N Q_M T) + N V_N J_{fp}^{N/2} \cos(N\theta) \; . \tag{4.25}$$

Here the phase is explicitly modulated by the term linear in the action I, as expected. Applying yet another generating function,

$$G_2(\theta, \bar{I}; T) = \theta \bar{I} + \frac{q}{Q_M} \cos(2\pi N Q_M T) \bar{I} \; , \tag{4.26}$$

shifts the modulation inside the angle dependence:

$$H_N(\bar{\theta}, \bar{I}; T) = \frac{N}{2}\alpha \bar{I}^2 + N V_N J_{fp}^{N/2} \cos\left[N\bar{\theta} + \frac{Nq}{Q_M} \cos(2\pi Q_M N T) \right] \; . \tag{4.27}$$

The cosine term can be expanded in Bessel functions J_m and harmonics via a variant of the Jacobi-Anger expansion of a plane wave,

$$\cos(A + B\cos C) = \sum_{m=-\infty}^{\infty} J_m(B)\cos(A + mC + m\pi/2) \ , \tag{4.28}$$

to produce a new Hamiltonian that has an infinite number of resonance terms:

$$H_N(\bar{\theta}, \bar{I}) = \frac{N}{2}\alpha\bar{I}^2 + NV_N J_{fp}^{N/2} \sum_{m=-\infty}^{\infty} J_m\left(\frac{Nq}{Q_M}\right)\cos(N\bar{\theta} + 2\pi m N Q_M T + m\pi/2) \ . \tag{4.29}$$

Examine a particle at non-zero $\bar{I}$ in the above Hamiltonian; there is a family of actions $\bar{I}_l$ (parameterized by an integer l) where a particle has a net phase advance of zero (modulo 1) over NT_M turns, or a tune of

$$Q_l = \frac{M}{N} + \frac{l}{N}Q_M \ . \tag{4.30}$$

The action that corresponds to this tune is $\bar{I}_l = \frac{2\pi l Q_M}{N\alpha}$. Now we can perform a sum over T_M N-turn periods near this tune if not much happens in that time (if $Q_M \ll Q_{\rm I}$) to find a new Hamiltonian that is autonomous over discrete time intervals of $T_M \cdot N$ turns. When this sum is performed, only one resonance ($m = -l$) remains since the others are suppressed in a similar manner to the resonance suppression before, and we find the Hamiltonian for $(T_M \cdot N)$-turn motion:

$$H_{N\cdot T_M}(\bar{\theta}, \bar{I}) = \frac{N}{2}T_M\alpha(\bar{I} - \bar{I}_l)^2 + NV_N J_{fp}^{N/2} T_M J_{-l}\left(\frac{Nq}{Q_M}\right)\cos(N\bar{\theta}) \ . \tag{4.31}$$

Note that this Hamiltonian contains a sideband resonance for every integer l; however the Bessel functions suppress the amplitudes of these sideband resonance strengths for large l since $J_{-l} \approx 0$ for $Nq/Q_M < |l|$. For the unsuppressed sidebands the Bessel functions can be approximated by

$$J_{-l}\left(\frac{Nq}{Q_M}\right) \approx \left(\frac{2Q_M}{N\pi q}\right)^{1/2} \cos\left(\frac{Nq}{Q_M} + \frac{l\pi}{4} - \frac{\pi}{4}\right) \ , \qquad \text{for } |l| < \frac{Nq}{Q_M} \tag{4.32}$$

with rms values $\sqrt{Q_M/N\pi q}$. This means that the $l = 1$ sideband suppressed and no sidebands are driven strongly if

$$q < \frac{Q_M}{N} \, . \tag{4.33}$$

Generally the k^{th} sideband is suppressed if $q < kQ_M/N$.

From the Chirikov overlap criterion (Chirikov 1979), sideband resonances overlap and local stochasticity results if $2I_W > I_{sep}$, where I_W is the sideband resonance island action half-width and I_{sep} is the action separation of the fixed points of neighboring sidebands. From the above formula for $\bar{I}_l$, it is apparent that $I_{sep} = 2\pi Q_M/N\alpha$. The island width must be calculated from Hamiltonian contour considerations and Equation (4.31) in the same fashion as the unperturbed primary resonance width calculation in Chapter 3; here it is found to be

$$I_W = 2\left[\frac{V_N J_{fp}^{N/2}}{\alpha} \, J_{-l}\left(\frac{Nq}{Q_M}\right)\right]^{1/2} \approx 2\left[\frac{V_N J_{fp}^{N/2}}{\alpha}\right]^{1/2} \left[\frac{Q_M}{N\pi q}\right]^{1/4} \tag{4.34}$$

for each sideband. Combining these with the overlap criterion and the definition of $Q_{\rm I}$ for the primary resonance (Equation [3.21]), sidebands overlap and chaos begins when

$$256 \; Q_{\rm I}^4 > N\pi q Q_M^3 \, . \tag{4.35}$$

Even though separatrices are destroyed and sidebands overlap when this condition is obeyed, the central regions of the primary resonances can still be locally stable for small enough Q_M, where adiabatic trapping takes over as in the previous discussion.

Lastly consider the nearly resonant case, $Q_M \approx Q_{\rm I}$, as described approximately by the linearized equations of motion. Equations (4.15) and (4.16) represent locally phase-locked motion only when the linearization of this motion around the fixed point in phase is a good approximation. This approximation fails when

$\sin(N\theta)$ becomes strongly nonlinear — that is, when $|N\theta| \approx 1$. This gives a weak constraint for bounded motion as

$$\left| \frac{qQ_M}{Q_M^2 - Q_{\rm I}^2} \right| < 1/N \ . \tag{4.36}$$

This constraint can be improved by including the next order (nonlinear) terms in the expansion of the driven pendulum equation (Tsironis 1990) but it is satisfactory in the resonant region where $Q_M \approx Q_{\rm I}$ and large motion is expected to become unbounded.

Summarizing, there are four basic constraints in the parameter space that divide the (q, Q_M) plane into four distinct regions. Near the driven pendulum resonance ($Q_M \approx Q_{\rm I}$), chaos occurs when

$$\left| \frac{qQ_M}{Q_M^2 - Q_{\rm I}^2} \right| > 1/N \ . \tag{4.37}$$

In the adiabatic regime ($Q_M \ll Q_{\rm I}$), chaos occurs when

$$|qQ_M| > \frac{Q_{\rm I}^2}{N} \ ; \tag{4.38}$$

below this threshold we have adiabatic stability of the fixed point and amplitude modulation dominates. In the fast-modulation approximation ($Q_M \gg Q_{\rm I}$) the k^{th} sideband appears when $q > |k|Q_M/N$. The first sideband off the primary resonance is then of non-negligible size when

$$q > \frac{Q_M}{N} \ ; \tag{4.39}$$

below this threshold there is stability with fast "phase modulation". The sidebands overlap and produce chaos when

$$256\ Q_{\rm I}^4 > N\pi q Q_M^3 \ . \tag{4.40}$$

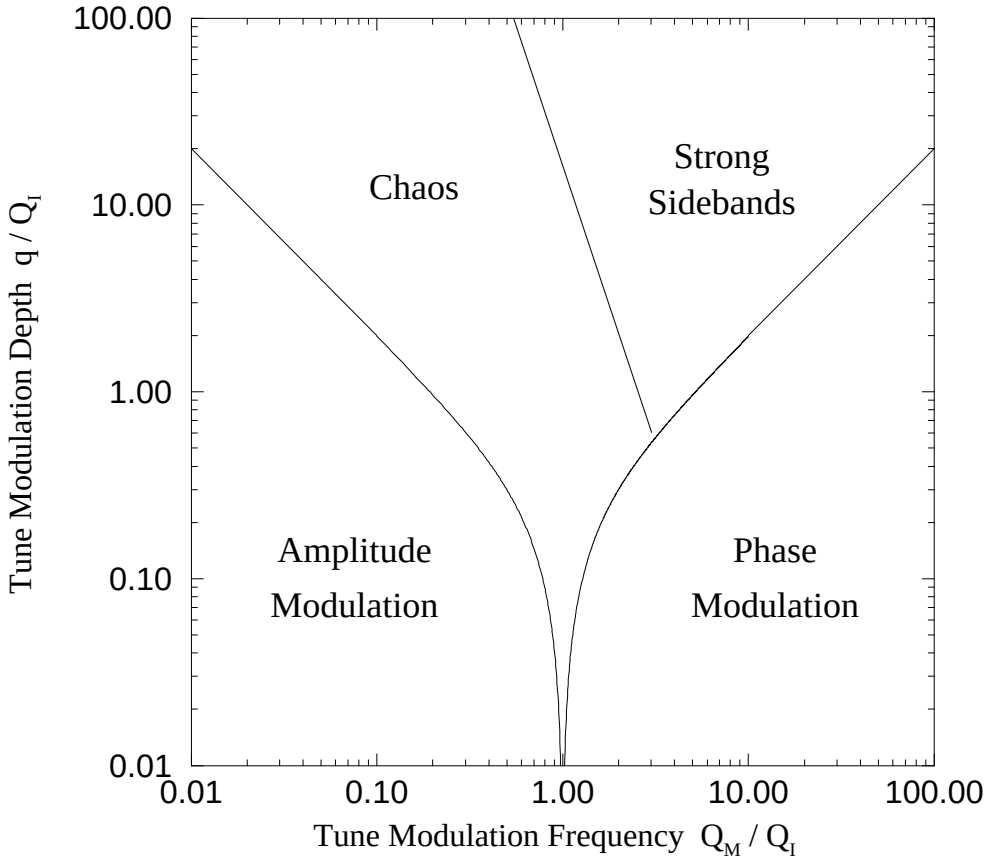

Figure 4.1: The (q, Q_M) parameter plane for $N = 5$, showing four distinct phases of motion. Local motion near the fixed point of the $5Q_x$ resonance is stable (i.e. phase-locked, or resonant) for all regions except "Chaos".

These regions of the tune modulation parameter plane (q, Q_M) and the lines separating them are shown in Figure (4.1).

The only tune modulation parameters that create detrapping of particles circling near the centers of nonlinear resonance islands are in the "Chaos" region of this figure, where there is expected to be no regular motion at all within the resonance island chain. It is important to note that with the presence of detuning and for purely one-dimensional motion, this chaotic region is localized. That is, the chaotic motion is restricted to a "thick layer" of stochasticity, covering the extent

of the overlapping sidebands created by the modulation. The presence of such a region does not necessarily prohibit stable motion at larger amplitudes if the detuning that is present is sufficiently strong to pull the tunes of particles at these amplitudes to nonresonant values. This is a contrast to "thin-layer" stochasticity, which is created by the overlap of thinner higher-order resonances in the vicinity of perturbed separatrices. For our purposes such thin-layer stochasticity can be ignored in this discussion, since the phase space extent of such regions is a great deal smaller than the extent of the chaotic band created by tune modulation.

The phase space of particles in each area of the tune modulation parameter plane is shown in Figure (4.2), plotted every modulation period. Shown on top for reference is the phase space of unperturbed particles, with $Q_{\mathrm{I}} = 6.1 \cdot 10^{-3}$ for the primary isolated $N = 5$ resonance shown. This is a nominally realistic value for Q_{I}, also similar to values found for small nonlinear strengths in tracking in the last chapter. Note that motion in the amplitude modulation and phase modulation regions is essentially indistinguishable from the unperturbed phase space and small-amplitude nonresonant motion is undisturbed in all cases. In the lower right figure the $k = 1$ sidebands can be seen on either side of the primary resonance, with stochasticity already beginning to form where the separatrices of the resonances overlap.

Alternative schemes to investigating the stability of the driven pendulum equation of motion (4.14) have been proposed which do not linearize the pendulum completely but including the first nonlinear terms in the expansion of the sine (Tsironis, Peggs and Chen 1990). Such an analysis predicts stability boundaries of the Mathieu equation, similar to the discussion of beta modulation in the next section. However these resonances are expected to be significantly weaker than the main driven pendulum resonance because they are found within the nonlinear response of the pendulum system.

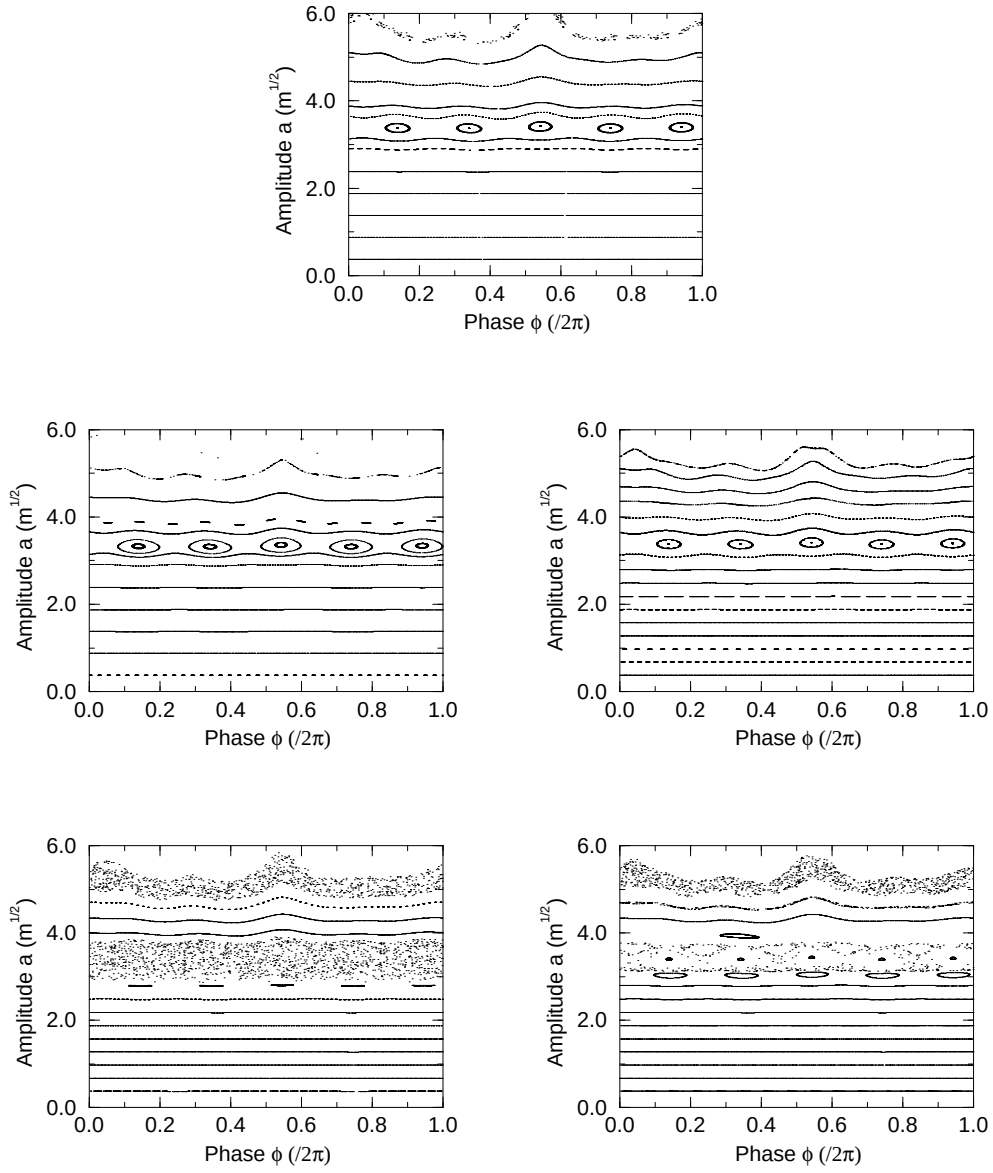

Figure 4.2: Phase spaces at various points in the (q, Q_M) tune modulation parameter plane as produced by the simulation program OdTrack for $N = 5$ resonance islands. Here the action $a = \sqrt{2J}$ is plotted against particle phase, for $Q_{\rm I} = 6.08 \cdot 10^{-3}$. From the top and left to right, the figures are described as: (a) The unperturbed phase space at $q = Q_M = 0$. (b) Amplitude modulation with $q = Q_M = Q_{\rm I}/10$. (c) Phase modulation with $q = Q_{\rm I}/10$, $Q_M = 10\,Q_{\rm I}$. (d) A thick stochastic band is produced in the chaos region with $q = Q_{\rm I}/2$, $Q_M = Q_{\rm I}$. (e) The first sideband ($k = 1$) appear at $q = 2Q_{\rm I}/5$, $Q_M = Q_{\rm I}/3$.

4.4 THE N–TURN HAMILTONIAN FOR BETA MODULATED 1–DIMENSIONAL RESONANCES

Now consider the one-turn one-dimensional Hamiltonian of Equation (3.13), representing the motion of a particle trapped in a nonlinear resonance island influenced by a small beta modulation (4.5):

$$H_1(\psi, J; t) = 2\pi Q J + \frac{1}{2}\alpha J^2 + V_N J^{N/2} \cos(N\psi) \left[1 + \frac{Nb}{2} \sin(2\pi Q_M t)\right] \ . \quad (4.41)$$

With the assumption that the tune is near an NQ resonance as before, quantified by stating that $Q = M/N + \delta_Q$, we can now go through the N-turn summing process to arrive at an N-turn version of this Hamiltonian:

$$\begin{aligned} H_N(\psi, J; T) = {} & 2\pi N \delta_Q J + \frac{N}{2}\alpha J^2 \\ & + N V_N J^{N/2} \cos(N\psi) \left[1 + \frac{Nb}{2} \sin(2\pi Q_M N T)\right] \ . \end{aligned} \quad (4.42)$$

The equations of motion given by this Hamiltonian show that neither the fixed point action nor phase are modulated by beta modulation — it is the depth of the oscillator well, or resonance strength, which is being modulated. Transforming to the coordinates (θ, I) is then not time-dependent, and can be accomplished using the linear canonical transformation of Equation (3.17). The Hamiltonian after this transformation has the form of a parametrically modulated nonlinear pendulum,

$$H_N(\theta, I; T) = \frac{N}{2}\alpha I^2 + N V_N J_{fp}^{N/2} \cos(N\theta) \left[1 + \frac{Nb}{2} \sin(2\pi Q_M N T)\right] \ . \quad (4.43)$$

Comparison of the relative effectiveness of tune modulation and beta modulation in detrapping particles within resonance islands and destroying persistent signals is more straightforward if we compare the respective equations of motion. The equation of motion for the angle of this oscillator in all ranges of modulation strength b and frequency Q_M is then

$$\ddot{\theta} = -N(2\pi Q_{\mathrm{I}})^2 \sin(N\theta) \left[1 + \frac{Nb}{2} \sin(2\pi Q_M N T)\right] \ . \quad (4.44)$$

The parametric form of the equation of motion is expected in the case of beta modulation because the strength of the resonance is being modulated as mentioned above, thus modulating both the island tune $Q_{\rm I}$ and the island width. The fixed point phases are not expected to change with beta modulation to any order, as can be seen by examining the above equation of motion when $\theta = 0$. From Equation (4.41) the equation for the fixed point action J_{fp} is

$$0 = 2\pi Q + \alpha J_{fp} + \frac{N}{2} V_N J^{\frac{N-2}{2}} \left[1 + \frac{Nb}{2} \sin(2\pi Q_M N T) \right] , \qquad (4.45)$$

indicating that this action is modulated in some complicated weak way.

The linearized form of Equation (4.44) is called the Mathieu equation. Conditions for the stability of such a parametrically driven oscillator have been described extensively in classical mechanics literature (Landau and Lifshitz 1975) and various tables of stability curves have been produced (Abromowitz and Stegun 1965, McLachlan 1951). The above form can be transformed to the canonical form cited in the literature,

$$\frac{d^2\theta}{dz^2} + [a - 2f \sin(2z)]\theta = 0 , \qquad (4.46)$$

noting the equivalences $z = N\pi Q_M$, $(Q_M/Q_{\rm I}) = 2/a^{1/2}$, and $b = \frac{f}{2N}\left(\frac{Q_M}{Q_{\rm I}}\right)^2$. Note that the modulation frequency still scales naturally with the island frequency, but the modulation strength b usurprisingly does not because it is not a natural frequency domain variable. For values of $b \ll 1$, resonances exist for the beta-modulated parametric oscillator when

$$Q_M(\text{resonant}) = \frac{2Q_{\rm I}}{k} \qquad (4.47)$$

where k is an positive integer. The strength of these resonances increases with increasing modulation strength b, but decreases with increasing k as b^k; the subharmonic resonance at $k = 1$ (or $Q_M = 2Q_{\rm I}$) is the strongest.

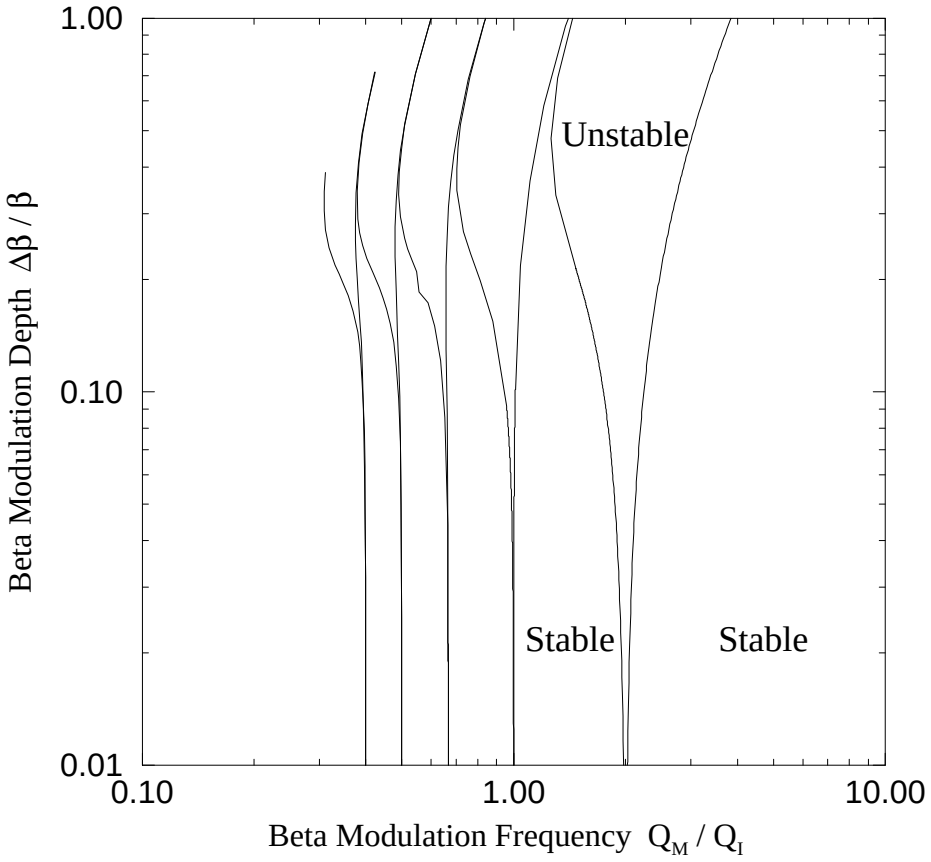

Figure 4.3: The $N = 5$ modulation parameter plane $(b, Q_M/Q_{\rm I})$ for beta function modulation, showing approximate widths for resonances of orders $k = 1$ to $k = 5$. Small oscillation stability is predicted below each set of resonance lines.

The $k = 1$ through $k = 5$ Mathieu resonances are shown in Figure (4.3), where motion within a resonance is expected to lead to instability of motion very close to the fixed point and subsequent detrapping. The $k = 1$ subharmonic resonance is evident at $Q_M = 2Q_{\rm I}$. All of the resonance widths typically grow non-negligible at a beta modulation depth of approximately $b \approx 0.10$. Higher order resonances are present but not shown for the sake of clarity. Note that in this stability diagram the vertical scale is $b = \frac{\Delta\beta}{\beta}$. Comparison of this figure to Figure (4.1) and recalling comments about the relative strengths of beta modulation and tune

modulation induced by a quadrupole error shows that tune modulation is on the order of $1/(10Q_{\mathrm{I}})$ times more effective than beta modulation in destroying local regular motion near the center of a nonlinear resonance island.

4.5 COMPARING HAMILTONIAN RESULTS TO SIMULATION

The entirety of this chapter concerns the phase-locking "stability" of particles trapped within nonlinear resonance islands subject to tune modulation and beta modulation. It is quite tedious to examine phase-space plots by hand for a variety of modulation conditions to determine the stability of the fixed-points, and so an algorithm was developed that allows fast and efficient location of fixed points in the two-dimensional map of the octupole-decapole lattice. This algorithm is quite easily extendible to any two-dimensional map.

Consider a fixed point in the phase space (x, x') at the location $(\bar{x}, \bar{x}')$. If this fixed point is elliptically stable a particle circulating around it will experience the linear transformation from initial coordinates (x, x') to $(x + \Delta x_1, x' + \Delta x_1')$

$$\begin{pmatrix} x + \Delta x_1 \\ x' + \Delta x_1' \end{pmatrix} = \begin{pmatrix} \bar{x} \\ \bar{x}' \end{pmatrix} + \begin{pmatrix} A & B \\ C & D \end{pmatrix} \begin{pmatrix} x - \bar{x} \\ x' - \bar{x}' \end{pmatrix} , \tag{4.48}$$

or

$$\begin{pmatrix} x + \Delta x_1 \\ x' + \Delta x_1' \end{pmatrix} = \begin{pmatrix} Ax - A\bar{x} + Bx' - B\bar{x}' + \bar{x} \\ Cx - C\bar{x} + Dx' - D\bar{x}' + \bar{x}' \end{pmatrix} . \tag{4.49}$$

The transformation matrix has the form of a rotation matrix if the motion around the fixed point is perfectly circular. For a more general elliptical fixed point, the trace of the rotation matrix is twice the cosine of the the total phase advance induced by the mapping; if this phase advance is denoted $2\pi Q_{\mathrm{I}} T$, where T is the number of turns tracked to produce one iteration of this map in Odfp, then

$$\cos(2\pi Q_{\mathrm{I}} T) = \frac{A + D}{2} . \tag{4.50}$$

This determines $Q_{\rm I}$ within an aliasing factor from the cosine once the transformation matrix elements are known, and this aliasing factor can be found by comparison of this $Q_{\rm I}$ to the theoretically predicted value.

Equation (4.49) only gives two constraints to find six unknowns, the fixed point location and the elements of the transformation matrix. Four other constraints are given by launching two more particles through the same mapping, offset by small amounts δx and $\delta x'$ in the x and x' directions respectively. The second particle experiences the linear transformation from $(x+\delta x, x')$ to $(x+\Delta x_2, x'+\Delta x_2')$:

$$\begin{pmatrix} x+\Delta x_2 \\ x'+\Delta x_2' \end{pmatrix} = \begin{pmatrix} Ax - A\bar{x} + Bx' - B\bar{x}' + \bar{x} + A\delta x \\ Cx - C\bar{x} + Dx' - D\bar{x}' + \bar{x}' + C\delta x \end{pmatrix} . \tag{4.51}$$

Subtracting the mapping equations for the first particle from those of the second gives equations for the matrix elements A and C:

$$A = \frac{\Delta x_2 - \Delta x_1}{\delta x} \qquad\qquad C = \frac{\Delta x_2' - \Delta x_1}{\delta x} . \tag{4.52}$$

Repeating the same process for a particle mapped from coordinates $(x, x'+\delta x')$ to $(x+\Delta x_3, x'+\Delta x_3')$ gives the other two matrix elements:

$$B = \frac{\Delta x_3 - \Delta x_1}{\delta x'} \qquad\qquad D = \frac{\Delta x_3' - \Delta x_1'}{\delta x'} . \tag{4.53}$$

Once the transformation matrix is known, Equation (4.49) can be inverted to find the fixed-points of the mapping:

$$\begin{pmatrix} \bar{x} \\ \bar{x}' \end{pmatrix} = \left[1 - \begin{pmatrix} A & B \\ C & D \end{pmatrix}\right]^{-1} \left[\begin{pmatrix} x+\Delta x_1 \\ y+\Delta x_1' \end{pmatrix} - \begin{pmatrix} A & B \\ C & D \end{pmatrix}\begin{pmatrix} x \\ x' \end{pmatrix}\right] . \tag{4.54}$$

This implies a matrix inversion — if this matrix inversion fails, then the initial conditions were such that the three particles were proceeding essentially linearly and there is no fixed point nearby.

This method has several advantages that make it extremely useful. It is extremely fast, requiring only three iteration about the local fixed point to assess

local motion, as opposed to minmax fixed-point location techniques where many hundreds of iterations must be performed. It is also very efficient and accurate; only two or three iterations of this procedure were required to find the fixed point of a particle even launched near the separatrix. And finally, it is very robust; anywhere in the two-dimesional phase space where there is local curvature created by the presence of a resonance island, this method will iterate. If such curvature is produced by proximity of a stable fixed point, the method will converge; conversely, if such curvature is produced by proximity of an unstable fixed point, this method will rapidly diverge.

The program Odfp is used to monitor local stability of a $5Q_x$ resonance island fixed point in the octupole-decapole lattice. For a given modulation tune Q_M, the fixed point was found for zero modulation strength. The modulation strength was then gradually increased and the local fixed point was again located, and the process was repeated until local motion was so distorted by the perturbation that no fixed point was found. This scan of modulation strengths was repeated for many tune modulation frequencies, and the points in the parameter space (q, Q_M) where the fixed point disappeared were plotted. Consecutive iterations with a variety of modulation strengths makes it possible to extrapolate fixed point locations through vertically thin regions of instability in some cases. However, for large regions of chaos merely the edges can be examined, as the strongly chaotic motion precludes any chance of finding fixed points.

The results of such a set of simulations for the case of tune modulation, with beta modulation explicitly absent, are shown in Figure (4.4). A point is plotted for each (q, Q_M) point where the fixed point was not found (or when local motion around the fixed point was not phase locked). The scan begins at $Q_M = 0.1\,Q_{\rm I}$, corresponding to a modulation period of approximately 1650 turns — searching further into the low-frequency adiabatic territory is constrained by available com-

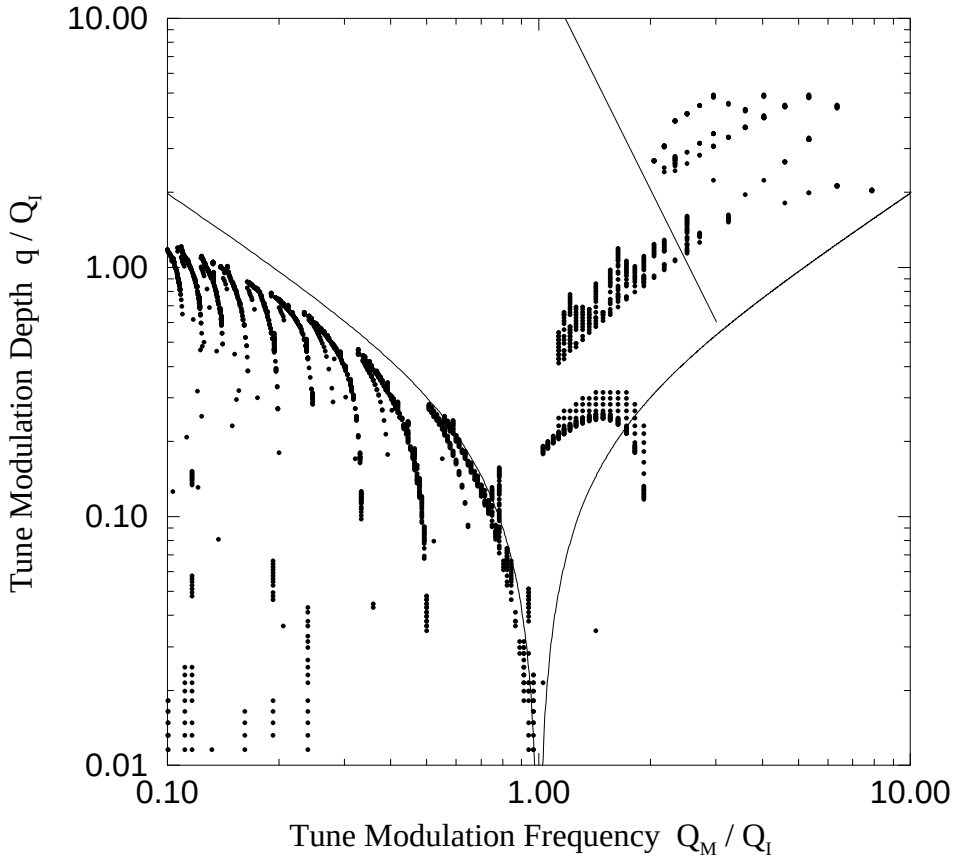

Figure 4.4: The (q, Q_M) parameter plane for $N = 5$, showing fixed point stability for a run of the tracking program Odfp. For this lattice $\tilde{b}_3 = 0.010$, $\tilde{b}_4 = 0.005$, $Q_{\rm I} = 0.0061$ and $1/Q_{\rm I} \approx 165$ turns. Lines from Figure (4.1) are shown for comparison to theory.

puter time and shows highly erratic behavior of many closely spaced resonances as described in the next paragraph. The frequency scan ends at $Q_M = 10\,Q_{\rm I}$, where the modulation period is approximately 16 turns and the approximation of modulation adiabaticity with respect to the turn time within the machine, $Q_M \ll 1$, begins to break down.

This figure shows the dominant $Q_M = Q_{\rm I}$ resonance, but also indicates that the stability border around this resonance is asymmetric. The low-frequency side of this resonance curves to low frequencies, and qualitatively agrees with the pre-

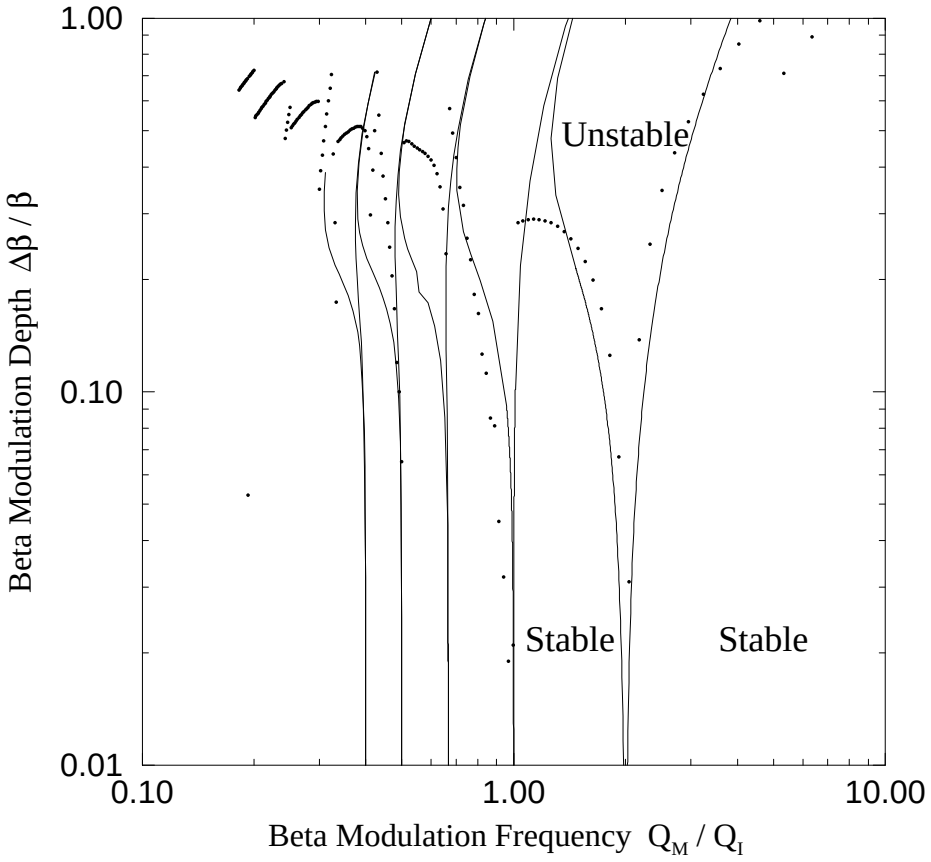

Figure 4.5: The (b, Q_M) parameter plane for $N = 5$, showing fixed point stability for a run of the tracking program Odfp. Tracking conditions were the same as those in Figure (4.4), and stability curves from Figure (4.2) are shown as solid lines for comparison.

dictions of tune modulation stability. However, the high-frequency side of this resonance appears almost vertical — at modulation frequencies just above the island tune, stability is greatly enhanced. This asymmetry is probably due to the higher order terms that have been neglected; indeed, the parametric oscillator displays such an asymmetry at this resonance (Landau and Lifshitz 1975). The presence of a cascade of thinner higher-order resonances at low frequencies, each dipping down at precisely the harmonics corresponding to Mathieu resonances, and the crescent-shaped instability region between $Q_M = Q_{\rm I}$ and the subhar-

monic resonance $Q_M = 2Q_{\rm I}$ also indicate that the nonlinear driven pendulum equation of motion (4.14) has weak instabilities defined by the Mathieu equation, as predicted elsewhere (Tsironis, Peggs and Chen 1990). At higher frequencies stability is shown up to large modulation strengths, on the order of values that would make the assumption that the tune modulation depth q is less than the difference between the base tune and the resonant tune false. There is indeed a large stable region in the area of "stable sidebands".

For beta function modulation a similar set of simulations were performed, with tune modulation absent, and the results of these simulations are shown in Figure (4.5). Resonance locations are exactly the same as predicted, though the behavior of tracking stability is somewhat different than that of the Mathieu predictions. This is quite reasonable because an approximation was made that $b \ll 1$ in the derivation of the Mathieu form for beta modulation, and so the predicted stability is expected to hold only for modulation levels much less than the beta function itself. Comparing the vertical scales between Figures (4.4) and (4.5) again shows that, for tune and beta modulation created by the same strength quadrupole ripple, tune modulation destroys the phase localization of resonance islands much more effectively.